Available online at www.sciencedirect.com

SCIENCE DIRECT®

Journal of Molecular Catalysis A: Chemical 207 (2004) 195–204

JOURNAL OF MOLECULAR CATALYSIS A: CHEMICAL

www.elsevier.com/locate/molcata

Theoretical and experimental study of NO/NO_2 adsorption over Co-exchanged type-A zeolite

Juan David Henao, Luis Fernando Córdoba, Consuelo Montes de Correa*

Department of Chemical Engineering, Universidad de Antioquia, Calle 67 No. 53-108, Medellín A.A. 1226, Colombia

Received 14 February 2003; received in revised form 2 July 2003; accepted 2 July 2003

Abstract

Adsorption of NO and NO_2 on cobalt exchanged type-A (Co-A) zeolite, has been studied by combining experimental and theoretical techniques. Adsorption energies were determined from temperature programmed desorption (TPD) measurements and ab initio calculations at the B3LYP/6-31G(d) level of theory. TPD profiles suggest that NO is disproportionated upon desorption on Co-A while NO_2 desorbs without transformation. An eight-atom cluster model of the transition metal and its closest environment in zeolite Co-A appears to qualitatively reproduce basic features of NO_x adsorption. Results from geometrical optimizations confirm that nitrogen monoxide (NO) is preferentially adsorbed through its nitrogen atom, whereas the two oxygen atoms of nitrogen dioxide (NO_2) appear to interact more favorably with Co-A. Upon NO adsorption on Co-A, a bent cobalt-mononitrosyl complex is formed. However, a negative charge is not developed on the nitrosyl and cobalt is not oxidized. Similarly, adsorption of nitrogen dioxide over Co-A does not change the oxidation state of cobalt. Theoretical calculations appear to reproduce the experimental adsorption energies within expected limits of error.

Keywords: Co-A zeolite; No_x; Adsorption energy; DFT calculations; TPD experiments

1. Introduction

Type A zeolites have been widely studied since they have been broadly applied as adsorbents and molecular sieves in chromatographic columns, separation of hydrocarbon mixtures, catalytic oxidation of propylene, and as driers for natural gas, refrigerants and organic solvents [1–3]. Transition metal ions in zeolite A have been studied because of their uniformity and open coordination. In particular, Co^{2+} ions in dehydrated zeolite A occupy trigonal sites near the six oxygen windows slightly recessed into the sodalite cages, but they can move out into the supercages when various molecules are bound by them [4–7]. The location and coordination of the Co^{2+} ions in zeolite A are unique with respect to the behavior of cobalt ions in other surfaces and complexes. Earlier reports [8,9] demonstrated that Co^{2+} cations in zeolite A are accessible to nitrogen monoxide (NO) and nitrogen dioxide (NO_2), two harmful pollutants generated from fossil fuel combustion. Later, Seff and coworkers [10] solved the structures of NO and NO_2 adsorbed on cobalt exchanged type-A (Co-A) zeolite (Si/Al $= 1$) from X-ray diffraction (XRD) measurements. They found that the mononitrosyl complex was favored and the calculated Co–NO angle was 141°. They also suggested the formation of NO^- species with the corresponding oxidation of three cobalt atoms in the unit cell, from Co^{2+} to Co^{3+}. Nevertheless, they noted that the bond length between cobalt and oxygen atoms in the zeolite framework was larger than that corresponding to a cobalt atom in its highest oxidation state. On the basis of IR and XPS studies of NO adsorbed on zeolite Co-A, Lunsford et al. [9] concluded that the nitrosyl ligand was neutral and cobalt was not oxidized. It was previously believed that if the M–N–O angle (where M stands for transition metal) in a coordination complex or M-zeolite was close to 180°, the nitrosyl species should be cationic whereas bent M–N–O complexes should be anionic. However, Enemark and Feltham [11] observed that the geometry (linear or bent) adopted by a NO group coordinated to a metal ion is not only governed by the charge. Other parameters such as the coordination number, the coordination geometry and the nature of the highest occupied molecular orbital should be considered. Hence, a direct relationship

* Corresponding author. Tel.: +574-210-5537; fax: +574-210-5537.
E-mail address: cmontes@quimbaya.udea.edu.co (C.M. de Correa).

1381-1169/$ – see front matter
doi:10.1016/S1381-1169(03)00501-6

between charge and geometry appears to be rather simplistic and may lead to wrong interpretations since other important factors may be disregarded. Therefore, it is unclear whether the observed bending of the Co–NO complex in zeolite Co-A, leads to an anionic mononitrosyl with the consequent oxidation of cobalt from Co^{2+} to Co^{3+}. This problem has never been addressed from a computational point of view.

Seff and coworkers [10] found that upon NO_2 adsorption on Co-A each Co^{2+} complexes one NO_2 molecule while its interaction with framework oxygen becomes weaker. They also reported that the adsorption complex with nitrogen directly bonded to cobalt, Co^{2+}–NO_2, was the dominant species formed. However, several authors have postulated that the oxygen atoms of NO_2 appear to interact with transition metals in zeolites [12–17]. Thus, local geometries and charge distributions of NO and NO_2 adsorption complexes on Co-A zeolite, are not completely understood and more insights are required. These important issues are addressed in this work by combining temperature programmed desorption (TPD) experiments and quantum chemistry calculations. The theoretical methods used here, have probed to be successful in studying adsorption and activation processes, reactivity and sitting of ions in zeolites [18–22], as well as, reproducing the local structure and the ligand field spectrum of cobalt in Co-A zeolite [23].

2. Experimental

2.1. Catalyst synthesis

The hydrothermal crystallization of the aluminosilicate type A was carried out in Teflon lined autoclaves according to a modified version of the procedure reported by Kerr [24]. The reactants employed were precipitated silica, trihydrated alumina, sodium hydroxide, tetramethylammonium hydroxide (TMAOH) pentahydrate (Aldrich), and distilled water. The required amount of sodium hydroxide was first dissolved in one-third of the water and then the trihydrated alumina was added under stirring and heating at 333 K. Subsequently, $TMAOH{\cdot}5H_2O$ was dissolved in the remaining water at 333 K and then silica was slowly added under stirring. The cloudy TMAOH-silicate gel was further stirred at room temperature for 1 h before adding the alumina slurry. The resulting aluminosilicate gel was homogenized by stirring during 3 h. The mole ratio of oxides in the gel was:

$$5TMA_2O : 1.5Na_2O : 4.5SiO_2 : Al_2O_3 : 100H_2O$$

After heating the autoclaves at 373 K in a forced convection oven for 20 h, they were removed from the oven and quenched in cold water. The resulting zeolite was separated from the mother liquor by vacuum filtration, washed with deionized water, dried at 333 K and calcined in air at 823 K for 3 h.

The XRD pattern and chemical analysis indicated that the resulting solid had the LTA structure. NH_4-A was obtained by overnight ion exchange of Na-A with 100 ml of a 1.0 M solution of NH_4Cl per gram of zeolite at 333 K. The solid was recovered by filtration and thoroughly washed with 2 L of deionized water. The NH_4-A material was further exchanged at 343 K with 100 ml/g of a 0.015 M solution of cobalt acetate for 12 h. After recovering the solid by filtration, it was thoroughly washed with deionized water and calcined at 673 K for 3 h in flowing air. Table 1 shows chemical analysis of synthesized Na-A, NH_4-A and Co-A, as well as, their BET surface areas. The cobalt exchange level reached about 90% while the Na/Al ratio was close to zero. From chemical analysis, the unit cell of synthesized Co-A zeolite has the following structural formula:

$$4Co^{2+}5.6H^{+}(9.6AlO_2 \cdot 14.4SiO_2 \cdot 16H_2O)$$

2.2. TPD analysis

The experimental adsorption energies were determined from temperature programmed desorption measurements. Two methodologies were used to collect TPD data:

i. 0.10 g of Co-A was loaded into a Pyrex reactor 9.5 mm i.d. and pretreated with 100 ml/min He at 773 K for 2 h. The sample was then saturated with either a mixture of 0.2% NO/He or 0.1% NO_2/He, flowing at 100 ml/min through the solid bed at a constant temperature of 303 K. Then, pure He was allowed to flow throughout the solid at 303 K in order to remove weakly adsorbed gas molecules. TPD experiments were carried out by heating the material at 5 K/min from 298 to 873 K in a 100 ml/min He stream. The resulting NO-TPD profile was analyzed using the method proposed by Niwa et al. [25] and Katada et al. [26], in order to calculate the NO adsorption energy.
ii. 0.10 g of Co-A was loaded into the same Pyrex reactor and pretreated with 100 ml/min He at 773 K for 2 h. Then, a mixture of 0.1% NO_2/He was adsorbed at 323 K until saturation and treated with pure He to remove physically

Table 1
Chemical composition and surface area of Na-A, NH_4-A and Co-A zeolites[a]

Sample	%Si	%Al	%Na	%Co	Si/Al	Na/Al	Co/Al	BET area (m^2/g)
Na-A	18.4	11.8	8.24	–	1.49	0.82	–	459.0
NH_4-A	19.4	12.4	1.46	–	1.50	0.14	–	440.9
Co-A	17.1	11.0	0.18	10.9	1.49	0.02	0.45	508.8

[a] Compositions in wt.%.

adsorbed NO_2. Desorption was conducted by heating the material at 5 K/min from 298 to 873 K in a 100 ml/min He stream. The whole procedure was repeated three more times at saturation temperatures of 373, 423 and 473 K. The model proposed by Leu and Chang [27] was used to evaluate the adsorption energy of NO_2.

The composition of gaseous mixtures was regulated by Brooks 5850E mass flow controllers. The amount of desorbed NO/NO_x was monitored by a chemiluminescence NO/NO_x analyzer ECO PHYSICS CLD 700 EL ht, connected in line with the reactor outlet. Temperature was controlled using an OMEGA temperature controller CN2042 model, using a K type thermocouple in contact with the zeolite bed. NO and NO_2 concentrations were recorded each second at the reactor outlet.

The mathematical models [25–27] used to evaluate the adsorption energies of NO and NO_2 from TPD profiles, give values which are taken as representative of the true integral heat of adsorption assuming thermodynamic equilibrium during desorption. Although both models will be used in this work, the Leu and Chang's model is expected to be the most accurate since there are fewer simplifications involved in its development [27].

3. Computational details

A simplified model of cobalt and its closest environment in zeolite A, with structural formula $Co(OH)_2H_2O$, has been adopted in this work. As shown in Fig. 1, it consists of a three-coordinated cobalt atom directly bonded to three oxygen atoms (from the framework of Co-A), which are bonded to hydrogen atoms, respectively, so the global cluster is neutral. First, the geometrical parameters of the model were set to match those determined by Seff and coworkers [10] for dehydrated zeolite Co-A, i.e. $R(\text{Co–O}) = 2.22$ Å and $\angle(\text{O–Co–O}) = 119.4^\circ$. The relative orientation of the terminal hydrogen atoms, as well as, their bond lengths to the oxygen atoms were established by optimization maintaining cobalt and oxygen atoms fixed. The model cluster in this stage will be further denoted as **Z** and its computationally determined energy will be referred as $E_{\mathbf{Z}}$.

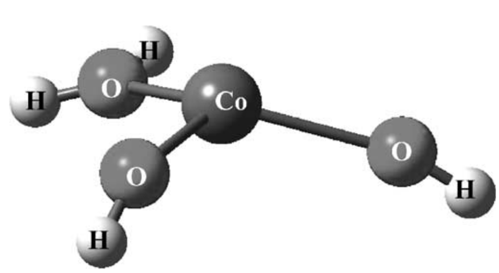

Fig. 1. **Z** model cluster ($Co(OH)_2H_2O$) used to represent a cobalt active site and its closest environment in zeolite Co-A.

Single molecules of NO and NO_2 were allowed to interact with the cobalt atom in the **Z** model and the structures were optimized in order to determine the equilibrium geometries for the most stable complexes. During optimizations, the cartesian coordinates of the oxygen atoms attached to cobalt were fixed whereas the remaining atoms were allowed to relax. The spin state of **Z** (the bare cobalt cluster), as well as, those of the NO and NO_2 adsorption complexes were determined by single point calculations at different multiplicities, according to the number of unpaired electrons. In the adsorption of NO, a mononitrosyl complex with triplet configuration was more stable than the corresponding structures in the singlet or quintet spin state. Similarly, the minimum electronic energy for the NO_2 adsorption complex, was also the structure in the triplet configuration with two unpaired electrons.

All single point (energy) calculations and geometrical optimizations were performed at the DFT level using the Gaussian 98 package [28], which uses Gaussian-type basis functions to describe molecular orbitals and charge density. B3LYP, the gradient corrected functional of Becke's three-parameter hybrid functional [29] and the correlation of Lee et al. [30], was used in all cases. The 6-31G(d) all-electron basis set available in Gaussian 98 was used to expand molecular orbitals. The default convergence criteria in Gaussian 98, was employed for geometry optimizations. To elucidate the preferred configurations adopted by NO and NO_2 upon adsorption, a single NO or NO_2 molecule was allowed to interact with a cobalt atom through their N or oxygen atoms. In this work, the structures in which nitrogen is directly bonded to cobalt will be denoted as **ON–Z** or **O$_2$N–Z**, whereas those in which oxygen atoms are attached to cobalt will be referred as **NO–Z** or **NO$_2$–Z**.

As pointed out by Lunsford et al. [9], the formation of dinitrosyl or highly coordinated $Co(NO)_y$ species in Co-A zeolite is unlikely due to strong repulsion forces which would be generated between nitrogen and lattice oxygen atoms, which are almost coplanar with cobalt. Therefore, dinitrosyl or highly coordinated species were not considered in this work. Electron diffraction, IR and XPS data [9,31] confirm that the NO adsorption complex on zeolite Co-A is mainly a bent mononitrosyl. Mingos [32] also suggests the simultaneous formation of linear mononitrosyl species. However, the exact nature of NO_2 adsorption complexes is less clear.

Natural bond orbital (NBO) population analysis [33,34] were carried out on the optimized structures to determine the occupancies (number of electrons assigned to orbitals in each atom) and charges of atoms in the adsorption complexes. The calculated N–O bond length for free gas NO, was 1.16 Å, in agreement with the experimental value of 1.15 Å [35]. Likewise, the calculated N–O bond distance and O–N–O angle for the NO_2 molecule were 1.20 Å and 133.8° in agreement with the experimental values of 1.19 Å and 133.9°, respectively [36]. Theoretical adsorption energies were determined according to the following equation:

$$\Delta E_{\mathrm{ADS}} = E_{\mathrm{AC}} - E_{\mathrm{NO}_x} - E_{\mathbf{Z}}$$

where ΔE_{ADS} represents the adsorption energy, E_{AC} the energy of the optimized adsorption complex, E_{NO_x} the energy of free NO or NO_2 molecule and $E_{\mathbf{Z}}$ the energy of **Z** (the bare Co-A model cluster). ΔE_{ADS} represents the total electronic energy as defined for the B3LYP/6-31G(d) model chemistry. It does not consider thermal corrections due to translational and electronic motions, vibrations or rotations (in the case of NO_2) [37].

4. Results and discussion

4.1. Experimental

The NO and NO_2 TPD profiles of Co-A are shown in Figs. 2(a–b) and 3(a–d). As can be seen in Fig. 2(a), most of adsorbed NO desorbs as NO_2, starting at 480 K and peaking at 562 K. The NO profile shows three small peaks at 350, 410 and 490 K, the first one is assigned to physically adsorbed nitrogen monoxide while the second one is likely due to NO adsorption on sites different from tricoordinated Co^{2+}. Upon adsorption of NO, a small fraction of cobalt Co^{2+} ions in Co-A zeolite can migrate from the usual exchange sites to more accessible positions and interact with the adsorbate [9]. NO can even form nitrosyl complexes with some of the residual sodium cations [38]. Both types of sites might be responsible for the NO peak at 410 K. The formation of NO_2 from NO takes place at high temperature over the Co^{2+} ions in normal exchange positions, i.e. the six-oxygen windows, as evidenced by the broad peak at 562 K. It might be the result of the disproportionation of NO to N_2O and NO_2 at high temperature. In the case of Co-FER, the disproportionation of NO has been observed in the 523–568 K range [39]. Because of the position of the high temperature peak for NO_2 in Fig. 2(a), we speculate that this peak is likely due

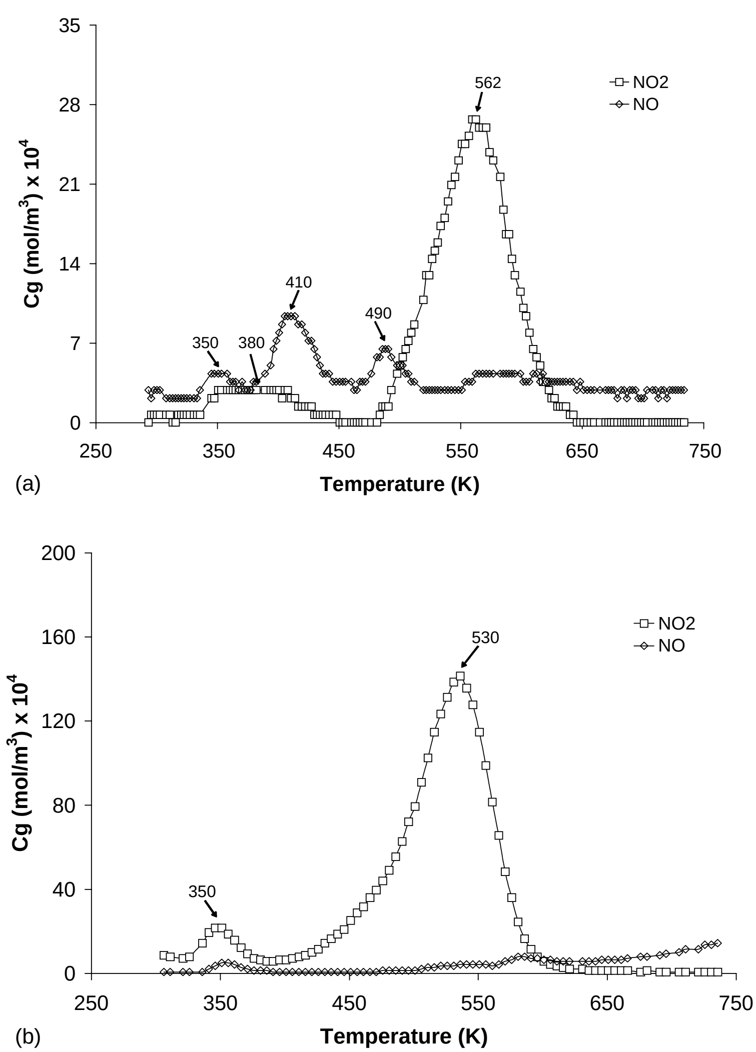

Fig. 2. NO and NO_2 TPD profiles on Co-A zeolite previously saturated with (a) 0.2% NO/He and (b) 0.1% NO_2/He. Temperature of saturation, 303 K; helium flow, 100 ml/min; heating rate, 5 K/min.

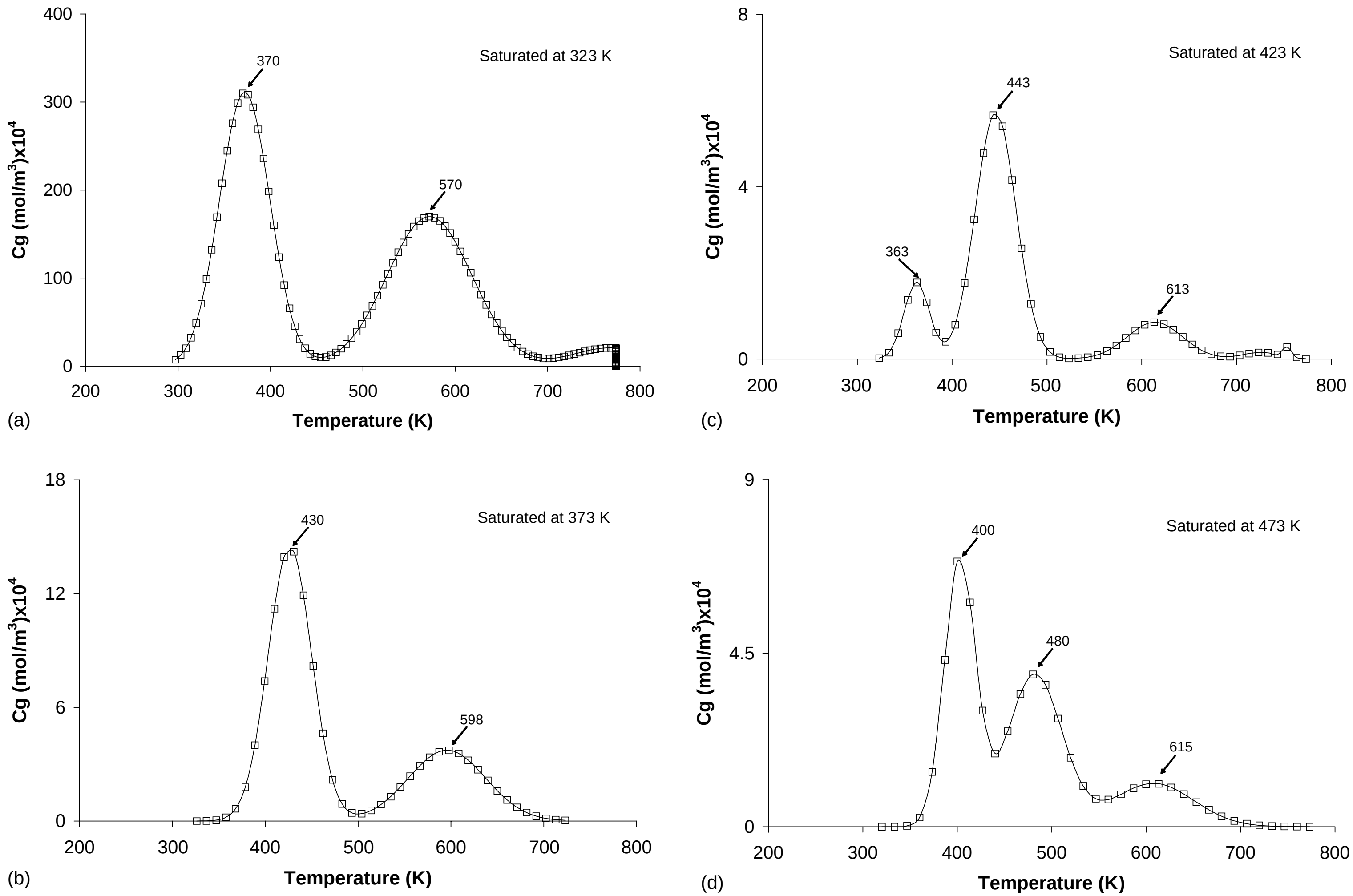

Fig. 3. NO_2 TPD profiles on Co-A zeolite previously saturated with 0.1% NO_2/He at (a) 323 K, (b) 373 K, (c) 423 K and (d) 473 K. Helium flow, 100 ml/min; heating rate, 5 K/min.

to NO_2 generated in the disproportionation of NO. Unfortunately, it was not possible to monitor N_2O formation with our analyzer. However, not all of adsorbed NO appears to be disproportionated. A portion of it seems to be simultaneously released when the formed NO_2 starts desorbing (see the peak at 490 K). The small NO_2 peak observed at 380 K in the nitrogen dioxide profile of Fig. 2(a) corresponds to physically adsorbed NO_2 which was probably introduced as an impurity in the NO/He flow used to saturate the sample. Fig. 2(b) shows that NO_2 desorbs unmodified. The small peak of NO observed around 355 K is likely due to impurities in the NO_2/He mixture used in the saturation process. The latter peak is assigned to physically adsorbed species while the broad peak at 530 K is associated to the chemically adsorbed nitrogen dioxide. Comparison between Fig. 2(a) and (b) shows that NO_2 molecules formed by disproportionation of NO desorb at higher temperatures as compared to those released from NO_2 adsorption. NO_2 starts desorbing at 490 K in Fig. 2(a), i.e. at 100 K higher temperature, than in Fig. 2(b). This shifting in the NO_2 desorption peak is an indirect evidence that the proposed disproportionation reaction is taking place, as each NO_2 molecule requires first to be formed before being released by the surface.

The method used to evaluate the adsorption energy of NO from the TPD profile in Fig. 2(a), considers equilibrium between gas phase and adsorbed species, as well as, readsorption during desorption [25,26]. The fulfilling of these assumptions depends on the nature of adsorbent and adsorbate, but also on the dynamical conditions under which the TPD experiments are carried out. In this work, the experimental conditions were chosen trying to match the requirements of the model. The thermodynamic background of the model accounts for the overall enthalpy and entropy changes involved in the desorption $\leftrightarrow$ adsorption process. Details regarding the application of the aforementioned method to NO_x adsorption on zeolite Co-A, has been given elsewhere [40]. It is important to notice that the model might not be accurate if any chemical transformation occurs during desorption. Because NO appears to undergo disproportionation during desorption over Co-A, its calculated experimental adsorption energy gives a rough estimate of the real integral heat. Notwithstanding, its numerical value is still representative, since it was obtained from the NO desorption profile, i.e. the fraction of released NO which did not disproportionate during the adsorption–desorption cycle. The experimental NO adsorption energy is compiled in the last row of Table 2.

The NO_2 adsorption energy has been determined from TPD profiles of Fig. 3(a–d) by using the Leu and Chang's model [27]. This model seems the most accurate under the present experimental conditions because it underlines a more direct relationship between Langmuir's adsorption model and integral heat of adsorption. From Fig. 3(a–d) it can be seen that the uptake of NO_2 decreases as the saturation temperature increases from 323 to 473 K. The basic features of the NO_2 TPD profile in Fig. 2(b) were reproduced in Fig. 3(a) and (b), i.e. the presence of two main peaks. The low temperature peak is assigned to physically adsorbed NO_2. The other one observed at a higher temperature is associated to chemisorbed species. Nevertheless, as the saturation temperature reached 423 K, see Fig. 3(c) and (d), the TPD profiles exhibit three peaks. Since peaks at 363 K in Fig. 3(c) and at 400 K in Fig. 3(d) appear at temperatures lower than those used to saturate the samples, they are assigned to nitrogen dioxide which was not completely evacuated after saturation. The second and third peaks in these figures are assigned to physically and chemically adsorbed NO_2 molecules. The position of these peaks appears to be shifted upwards as the saturation temperature increases. Particularly, shifts observed in the chemisorption peaks suggest that chemisorption becomes more selective with saturation temperature and only a small fraction of the cobalt ions is able to bind NO_2 with the required strength. The decreasing intensity of the peak assigned to chemisorbed NO_2 with increasing temperature supports this observation. The experimental NO_2 adsorption energy calculated from data of Fig. 3(a–d) is compiled in the last row of Table 4.

4.2. Computational

Fig. 4(a) and (b) illustrate two schemes of NO interaction with the **Z** cluster. Table 2 lists the geometrical parameters associated with both complexes in the second and third

Table 2
Geometrical parameters and adsorption energies of NO adsorption complexes on the cluster model **Z** and zeolite Co-A

	NO–**Z**	ON–**Z**	ON–Co-A zeolite[a]	Deviation (%)	NO gas
Co–O(1) (Å)	2.22	2.22	2.22	0	–
Co–N (Å)	–	1.94	2.23	13	–
N–O(2) (Å)	1.17	1.13	1.47	23	1.16
O(1)–Co–N (°)	–	101.3	100.2	1	–
Co–N–O(2) (°)	–	142.1	141.0	1	–
O(1)–Co–O(1) (°)	116.8	116.8	116.9	0	–
ΔE_{ADS} (kJ/mol)	−115.8[b]	−193.1[b]	−158.5[c]	–	–

[a] Parameters of NO adsorbed on zeolite Co-A; taken from [10].
[b] Computationally calculated.
[c] Experimentally determined from TPD data in Fig. 2(a).

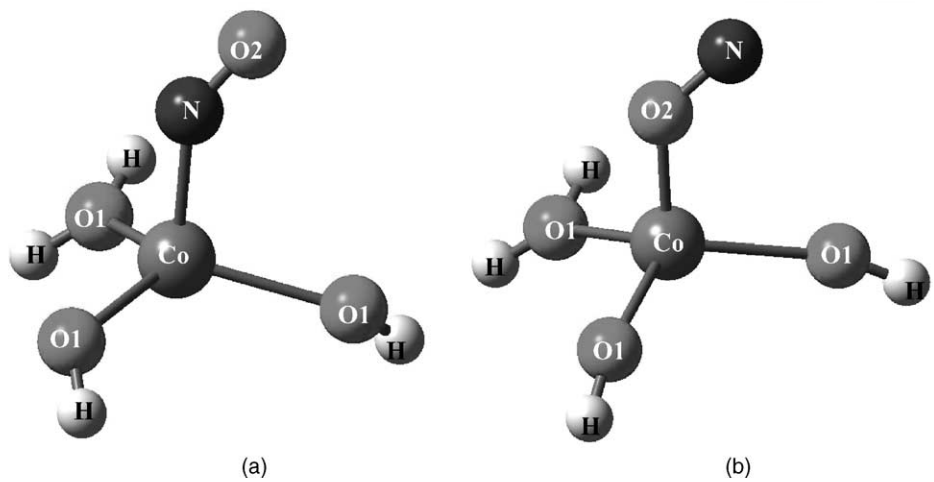

Fig. 4. Schematic representation of NO adsorption complexes on the model cluster **Z**. (a) Cobalt binding nitrogen (**ON**–**Z**) and (b) cobalt binding oxygen (**NO**–**Z**).

columns and in the last row the theoretical adsorption energies are compiled. Comparison between the **NO**–**Z** and **ON**–**Z** adsorption energies shows that the adsorption energy of **ON**–**Z** complex is 77.3 kJ/mol more stable than **NO**–**Z**. This energy difference confirms that the mononitrosyl complex becomes the preferred species upon NO adsorption on Co-A. Experimental observations agree with this theoretical result [9,10,31,32]. The percent deviation between the calculated geometry parameters in the **ON**–**Z** complex and those experimentally determined by Seff and coworkers [10] are listed in Table 2 (column 5). The simplified **ON**–**Z** model is able to reproduce the mononitrosyl bending, as well as, other angles among different centers in the cluster but, fails predicting the Co–N and N–O bond lengths. Although the experimental bond lengths are average values obtained by considering that Si–O and Al–O interatomic distances are the same in Co-A zeolite [10], the deviations appear to be much higher than the inherent uncertainty in the experimental values. The high underestimation of these bonds (13% error for Co–N and 23% error for N–O), may be due to the small size of the model cluster used.

Table 3 presents the results of NBO analysis for the **NO**–**Z** and **ON**–**Z** complexes. These results suggest that interactions between NO and cobalt do not modify the oxidation state of cobalt. Cobalt in the bare **Z** cluster has a formal charge of +1.66 (Q_{Co} in Table 3) and a $3d^7$ electronic distribution, indicating that its oxidation state is +2 as experimentally observed [5–9]. After interacting with NO, a strong reorganization of the Co electronic population occurs but, its electronic structure does not change ($4s^{0.3}$ $3d^{7.2}$), indicating that cobalt is not oxidized. At the same time, there is a small negative charge transfer from NO towards the cluster but, it is not as significant as to become the nitrosyl complex of cationic nature. IR experimental results of NO adsorption on zeolite Co-A [9], demonstrate a minimum electron donation towards the nitrosyl ligand.

Charge transfer has been recognized as an effective way to activate the N–O bond since it concentrates more electrons in the NO antibonding π orbitals [41]. The NO molecule which adds an unpaired electron to its antibonding 2π shell, may donate its unpaired electron to the metal center forming a NO^+ ligand with a stronger intramolecular bond or may accept an electron forming a weakly NO^- ligand [21]. These two situations are limiting cases, but in general a polarized N–O bond will be formed depending on the nature of the transition metal and its host matrix. Previous results [11] indicate that a bent mononitrosyl complex in Co-A zeolite is possible, even though the nitrosyl species does not carry a negative charge nor oxidation of cobalt does occur. In other words, charge does not determine the mononitrosyl geometry in zeolite Co-A.

In the case of NO_2 adsorption on Co-A, the geometrical parameters for the two complexes, as well as, their adsorption energies are compiled in Table 4. Fig. 5(a) and (b) illustrate the structures of the adsorption complexes obtained after geometrical optimization. Upon adsorption of NO_2, the N–O bond distance is enlarged from 1.20 to 1.23 Å while the O–N–O angle is reduced from 133.8 to 108.0°,

Table 3
Electronic population of cobalt and charges derived from NBO analysis of the NO adsorption complexes over the model cluster **Z**

	Q_{NO}	Q_{co}	4sp	3dxy	3dxz	3dyz	$3dx^2–y^2$	$3dz^2$
NO + **Z**	0.00	+1.66	0.27	1.32	1.63	1.79	1.29	1.04
NO–**Z**	+0.08	+1.61	0.32	1.35	1.61	1.67	1.39	1.08
ON–**Z**	+0.26	+1.50	0.32	1.46	1.63	1.53	1.38	1.19

Table 4
Geometrical parameters and adsorption energies of NO_2 adsorption complexes on the cluster model **Z** and zeolite Co-A

	O_2N–Z	NO_2–Z	O_2N–Co-A zeolite[a]	NO_2 gas
Co–O(1) (Å)	2.15	2.15	2.15	–
Co–N (Å)	2.07	–	1.95	–
Co–O(2) (Å)	–	2.22	–	–
N–O(2) (Å)	1.28	1.23	1.09	1.20
N–O(3) (Å)	1.28	–	1.27	1.20
Co–N–O(2) (°)	133.1	–	125.0	–
Co–N–O(3) (°)	133.9	–	147.0	–
O(2)–N–O(3) (°)	93.0	108.0	88.0	133.8
O(1)–Co–O(1) (°)	114.7	114.7	114.6	–
ΔE_{ADS} (kJ/mol)	29.6[b]	−57.7[b]	−44.3[c]	–

[a] Parameters of NO_2 adsorbed on zeolite Co-A; taken from [10].
[b] Theoretically computed.
[c] Experimentally determined from TPD profiles in Fig. 3.

evidencing a small activation of the molecule. Comparison between the calculated theoretical adsorption energies for **O_2N–Z** and **NO_2–Z**, show that the latter complex is more stable than the former by 87.3 kJ/mol. Besides, the calculated adsorption energy for **O_2N–Z** is positive, indicating that it is unstable with respect to the zeolite and the NO_2 gas molecule. Therefore, NO_2 appears to interact with cobalt in zeolite Co-A through its two oxygen atoms. This behavior of nitrogen dioxide has also been observed in other transition metal-zeolite systems [12–17,42], even though Li et al. [43] proposed that both species, i.e. O_2N–Co-zeolite and NO_2–Co-zeolite can be formed on Co-FER. Because the structures for the most stable adsorption complex proposed by XRD (**O_2N–Z**) and DFT calculations (**NO_2–Z**) are completely different, comparison of geometrical parameters for the two NO_2 adsorption complexes in Table 4 is not relevant.

NBO calculations for the two NO_2 complexes are presented in Table 5. The initial electronic configuration of cobalt corresponds to Co^{2+}. After interacting with NO_2 its electronic population, mainly the 3dyz, $3dx^2$–y^2 and $3dz^2$ orbitals, is rearranged but, its oxidation state does not change. A small charge transfer from cobalt to framework oxygen atoms, equivalent to 0.04*e*, can be calculated as the difference between the amount of charge transfer from NO_2 to Co^{2+} and the amount of cobalt charge gain.

The **Z** model cluster used in this work qualitatively represents the transition metal centers, allowing to get some insight about the molecular process involved in the adsorption of NO and NO_2 on Co-A. A good representation of the interatomic angles in the NO adsorption complex is achieved. Even more important, the model is able to reproduce the experimental observations that mononitrosyl complex bending does not necessarily lead to development of a negative charge in NO or change the oxidation state of Co^{2+}. The model also reproduces the experimental observation that NO_2 prefers to interact with cobalt through its oxygen atoms. The theoretical values of the adsorption energies tabulated in the last rows of Tables 2 and 4 appear to

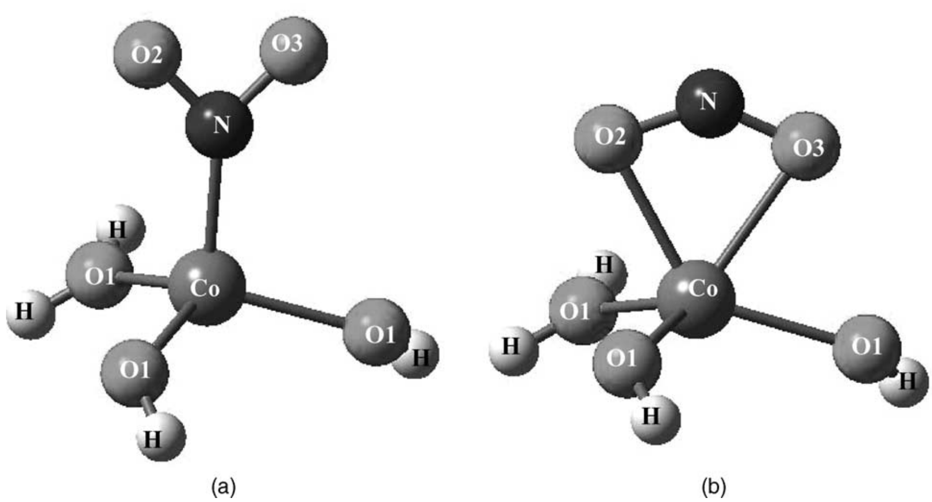

Fig. 5. Schematic representation of NO_2 adsorption complexes on the model cluster **Z**. (a) Cobalt binding nitrogen (**O_2N–Z**) and (b) cobalt binding oxygen atoms (**NO_2–Z**).

Table 5
Electronic population of cobalt and charges derived from NBO analysis of the NO_2 adsorption complexes over the model cluster **Z**

	Q_{NO_2}	Q_{Co}	4sp	3dxy	3dxz	3dyz	$3dx^2$–y^2	$3dz^2$
NO_2 + **Z**	0.00	+1.66	0.27	1.32	1.63	1.79	1.29	1.04
NO_2–Z	+0.11	+1.59	0.35	1.21	1.68	1.17	1.66	1.39
O_2N–Z	+0.09	+1.61	0.32	1.72	1.70	1.32	1.14	1.26

Table 6
Comparison between the theoretical adsorption energies computed in this work and those reported for NO and NO_2 adsorption on Co-ZSM-5

Model cluster	ΔE_{ADS} (kJ/mol)
ON–Z	−193.1
NO adsorption complex[a]	−182.0
NO_2–Z	−57.7
NO_2 adsorption complex[b]	−56.9

[a] From [44].
[b] From [12].

be overestimated as compared to those obtained experimentally, even though they are of the same order of magnitude. Since the tabulated theoretical energy is just the SCF electronic energy, the estimation can be improved by making two corrections: the basis set superposition error correction, which might account for ca. 10–20% of the reported value and the thermal correction (translation motion, vibrations, rotations and electronic motion) which might account for ca. 3–7% of the reported value. Both corrections would decrease the absolute value of the electronic adsorption energy [37], diminishing the discrepancy between experimental and theoretical adsorption energies.

Table 6 compares theoretical adsorption energies calculated in this work and other reported for Co-zeolites [12,44]. Overall, the agreement is satisfactory considering the simplicity of the model cluster used. A cluster able to account for the steric effects of molecules adsorbed on different sites and the electrostatic effect of compensation cations like Na^+ remaining after ion-exchange, would generate better estimates of adsorption energies. The computational costs however, would also dramatically increase.

5. Conclusions

A fraction of the NO adsorbed on Co-A zeolite appears to be disproportionated into NO_2 and N_2O. NO_2 from the disproportionation reaction desorbed at 562 K whereas the remaining NO is released by the surface at 490 K. In contrast, NO_2 does not appear to undergo chemical transformation during its adsorption–desorption cycle on Co-A. The model cluster used in the theoretical calculations, leads to a first approximation of the molecular process involved in NO and NO_2 adsorption over Co-A zeolite. Upon NO adsorption, a bent mononitrosyl complex is formed but, neither no negative charge is developed in the nitrosyl species nor oxidation of cobalt appears to take place. This suggests that charge and geometry of the nitric oxide adsorption complex are not necessarily dependent each other. On the other side, cobalt in zeolite Co-A prefers to interact with the two oxygen atoms of nitrogen dioxide, rather than with the nitrogen atom. Furthermore, adsorption of nitrogen dioxide over Co-A does not change the oxidation state of cobalt.

Acknowledgements

Authors are grateful to Universidad de Antioquia, for financially supporting this work.

References

[1] D.M. Ruthven, Chem. Eng. Progr. 84 (1988) 42.
[2] D.E.W. Vaughan, Chem. Eng. Progr. 84 (1988) 25.
[3] H. Lee, L. Kevan, J. Phys. Chem. 90 (1986) 5776.
[4] K. Klier, P. Hutta, R. Kellerman, ACS Symp. Ser. 40 (1977) 108.
[5] P.E. Riley, K. Seff, J. Phys. Chem. 79 (1975) 1594.
[6] K. Klier, J. Am. Chem. Soc. 91 (1969) 5392.
[7] P.E. Riley, K. Seff, J. Chem. Soc. Chem. Commun. (1972) 1287.
[8] P.E. Riley, K. Seff, Inorg. Chem. 13 (1974) 1355.
[9] J.H. Lunsford, P.J. Huta, M.J. Lin, K.A. Windhorst, Inorg. Chem. 3 (1978) 606.
[10] W.V. Cruz, P.C.W. Leung, K. Seff, Inorg. Chem. 18 (1979) 1692.
[11] J.H. Enemark, R.D. Feltham, Coord. Chem. Rev. 13 (1974) 339.
[12] A. Sierraalta, R. Añez, M.-R. Brussin, J. Catal. 205 (2002) 107.
[13] L. Rodríguez-Santiago, M. Sierka, V. Branchandell, M. Sodupe, J. Sauer, J. Am. Chem. Soc. 120 (1998) 1545.
[14] X. Solans-Monfort, V. Branchandell, M. Sodupe, J. Phys. Chem A. 104 (2000) 3225.
[15] R.W. Joyner, M. Stockenhuber, Catal. Lett. 45 (1997) 15.
[16] K.A. Windhorst, J.H. Lunsford, J. Am. Chem. Soc. 97 (1974) 1407.
[17] B.J. Adelman, T. Beutel, G.-D. Lei, W.M.H. Sachtler, J. Catal. 158 (1996) 327.
[18] H. Himei, M. Yamada, M. Kubo, R. Vetrivel, E. Broclawik, A. Miyamoto, J. Phys. Chem. 99 (1995) 12461.
[19] W.F. Schneider, K.C. Hass, R. Ramprasad, J.B. Adams, J. Phys. Chem. B. 102 (1998) 3692.
[20] G.M. Zhidomirov, A.L. Yakovlev, M.A. Milov, N.A. Kachurovskaya, I.V. Yudanov, Catal. Today 51 (1999) 397.
[21] E. Broclawik, J. Datka, B. Gil, W. Piskors, P. Kozyra, Topics Catal. 11/12 (2000) 335.
[22] S.A. MacMillan, L.J. Broadbelt, R. Snurr, J. Phys. Chem. B. 106 (2002) 10864.
[23] K. Pierloot, A. Delabie, C. Ribbing, A.A. Verberckmoes, R.A. Schoonheydt, J. Phys. Chem. B. 102 (1998) 10789.
[24] G. Kerr, J. Chem. Soc. 971 (1961) 1537.
[25] M. Niwa, N. Katada, M. Sawa, Y. Murakami, J. Phys. Chem. 99 (1995) 8812.
[26] N. Katada, H. Igi, J.-H. Kim, M. Niwa, J. Phys. Chem. B. 101 (1997) 5969.
[27] F.-C. Leu, T.-H. Chang, in: Proceedings of the 17th North American Catalysis Society Meeting, vol. 1, NACS, 2001, pp. 1–2.
[28] M.J. Frisch, G.W. Trucks, H.B. Schlegel, G.E. Scuseria, M.A. Robb, J.R. Cheeseman, V.G. Zakrzewski, J.A. Montgomery Jr., R.E. Stratmann, J.C. Burant, S. Dapprich, J.M. Millam, A.D. Daniels, K.N. Kudin, M.C. Strain, O. Farkas, J. Tomasi, V. Barone, M. Cossi, R. Cammi, B. Mennucci, C. Pomelli, C. Adamo, S. Clifford, J. Ochterski, G.A. Petersson, P.Y. Ayala, Q. Cui, K. Morokuma, D.K. Malick, A.D. Rabuck, K. Raghavachari, J.B. Foresman, J. Cioslowski, J.V. Ortiz, A.G. Baboul, B.B. Stefanov, G. Liu, A. Liashenko, P. Piskorz, I. Komaromi, R. Gomperts, R.L. Martin, D.J. Fox, T. Keith, M.A. Al-Laham, C.Y. Peng, A. Nanayakkara, M. Challacombe, P.M.W. Gill, B. Johnson, W. Chen, M.W. Wong, J.L. Andres, C. Gonzalez, M. Head-Gordon, E.S. Replogle, J.A. Pople. Gaussian 98, Revision A.9, Gaussian Inc., Pittsburgh, PA, 1998.
[29] A.D. Becke, J. Chem. Phys. 98 (1993) 5648.
[30] C. Lee, W. Yang, R.G. Parr, Phys. Rev. B 37 (1988) 785.
[31] K. Seff, Acc. Chem. Res. 9 (1976) 121.
[32] D.M.P. Mingos, Inorg. Chem. 12 (1973) 1211.

[33] E.D. Glendening, A.E. Reed, J.E. Carpenter, F. Weinhold, NBO Version 3.1, Gaussian 98, Revision A.9, Gaussian Inc., Pittsburgh, PA, 1998.
[34] A.E. Reed, L.A. Curtiss, F. Weinhold, Chem. Rev. 88 (1988) 899.
[35] F. Wang, F.P. Larkins, J. Phys. B. 31 (1998) 3789.
[36] Y. Morino, M. Tawimoto, S. Saito, E. Hirota, R. Awata, T. Tanaka, J. Mol. Spectrosc. 98 (1983) 331.
[37] D.A. McQuarrie, Statistical Mechanics, Harper & Row, New York, 1973.
[38] A. Pöppl, T. Rudolf, P. Manikandan, D. Goldfarb, J. Am. Chem. Soc. 122 (2000) 10194.
[39] Y. Li, J.N. Armor, J. Catal. 150 (1994) 376.
[40] J.D. Henao, Estudio teórico-experimental de la reducción de óxidos de nitrógeno con zeolitas metálicas, M.Sc Thesis, Universidad de Antioquia, Medellín, 2002, pp. 26–38.
[41] K. Klier, R.G. Herman, S. Hou, Stud. Surf. Sci. Catal. 84 (1994) 1507.
[42] X. Wang, H.-Y. Chen, W.M.H. Sachtler, J. Catal. 197 (2001) 281.
[43] Y. Li, T.L. Slager, J.N. Armor, J. Catal. 150 (1994) 388.
[44] K. Yajima, Y. Ueda, H. Tsuruya, T. Kanougi, Y. Oumi, S.S.C. Ammal, S. Takami, M. Kuba, A. Miyamoto, Appl. Catal. A. 194–195 (2000) 183.